



Article

Analyzing Driving Factors of Drought in Growing Season in the Inner Mongolia Based on Geodetector and GWR Models

Bowen Ji ¹, Yanbin Qin ^{1,*}, Tingbin Zhang ^{1,2} , Xiaobing Zhou ³ , Guihua Yi ⁴ , Mengting Zhang ¹ and Menglin Li ¹

¹ College of Earth Science, Chengdu University of Technology, Chengdu 610059, China

² State Environmental Protection Key Laboratory of Synergetic Control and Joint Remediation for Soil & Water Pollution, Chengdu University of Technology, Chengdu 610059, China

³ Geological Engineering Department, Montana Technological University, Butte, MT 59701, USA

⁴ College of Tourism and Urban-Rural Planning, Chengdu University of Technology, Chengdu 610059, China

* Correspondence: qinyanbin@cdu.cn

Abstract: As an important ecological security barrier in northern China, the Inner Mongolia Autonomous Region (hereinafter referred to as Inner Mongolia) is seriously affected by drought. It is of great significance to characterize the spatial distribution of drought and identify the influencing factors of drought. Due to complex interactions among drought driving factors, it is difficult to quantify the contribution of each driving factor to drought using linear correlation analysis alone. In this study, we used the Standardized Precipitation Evapotranspiration Index (SPEI) as a quantitative indicator of drought to discuss the spatiotemporal variation of drought during growing seasons in the Inner Mongolia from 2000 to 2018. We quantitatively characterized mode, scope, and intensity of changes in SPEI caused by drought-influencing factors such as weather, water, topography, soil, and human activities using the Geodetector and Geographically Weighted Regression (GWR) models. We concluded that about 20.3% of the region showed a downward trend in SPEI, with the fastest rate of decline in the central and western Inner Mongolia. Air temperature, precipitation, elevation, and distance to rivers are the main controlling factors in drought change, and the factor interactions showed nonlinear enhancement. The drought driving effect was obvious in Alxa League, Wuhai City, Ulanqab City, and Baotou City. The results will help us to understand the effects of the driving factors on drought and eventually help policymakers with water-resource management.

Keywords: growing season; driving factors of drought; Geodetector; GWR model; Inner Mongolia



Citation: Ji, B.; Qin, Y.; Zhang, T.; Zhou, X.; Yi, G.; Zhang, M.; Li, M. Analyzing Driving Factors of Drought in Growing Season in the Inner Mongolia Based on Geodetector and GWR Models. *Remote Sens.* **2022**, *14*, 6007. <https://doi.org/10.3390/rs14236007>

Academic Editor: Giorgio Baiamonte

Received: 15 October 2022

Accepted: 23 November 2022

Published: 27 November 2022

Publisher's Note: MDPI stays neutral with regard to jurisdictional claims in published maps and institutional affiliations.



Copyright: © 2022 by the authors. Licensee MDPI, Basel, Switzerland. This article is an open access article distributed under the terms and conditions of the Creative Commons Attribution (CC BY) license (<https://creativecommons.org/licenses/by/4.0/>).

1. Introduction

As one of the most serious meteorological and environmental disasters, drought can severely impact the natural environment, crop production, social economy, and human life, but its impact mode is not easy to be quantified [1]. The Sixth Assessment Report (AR6) of the Intergovernmental Panel on Climate Change (IPCC) points out that in the past 30 years, the global average temperature has increased by 1.5 °C, extreme climate events occur frequently, and the degree of drought will continue to increase in the future. Drought impacts species and structure of vegetation. It is an important factor affecting vegetation growth, vegetation restoration, and soil desertification [2–4]. Changes in hydrothermal conditions can lead to biomass loss and ecosystem destruction. Therefore, investigating the spatiotemporal variation of drought during the growing season (from April to September) in Inner Mongolia, identifying causes of drought, and separating and quantifying relative contributions of the controlling factors of drought are of practical significance for drought remediation and ecosystem restoration.

Due to uncertainties in starting and ending times, spatial scale, time lag effects, and other factors of drought events, researchers mainly monitor and analyze drought effects through a series of drought indicators [1,5]. The Palmer Drought Severity Index (PDSI)

is the most widely used water-balance-based meteorological drought index, which comprehensively considers water supply and demand. However, it has limitations in judging short-term droughts [6]. The Standardized Precipitation Index (SPI) calculates the probability of precipitation distribution; however, it is difficult to handle the task of meteorological drought monitoring under the context of global change [7]. The Standardized Precipitation Evapotranspiration Index (SPEI) leverages the advantages of PDSI and SPI [8,9]. It not only considers the balance of water and energy, but also reflects the deficit and accumulation process of surface water. Therefore, it is widely used in climate studies [7,10], agriculture [11], hydrology [12,13], and so on. At the same time, SPEI can be calculated at multiple time scales. SPEI-3, used to characterize drought in a seasonal scale, reflects short-term regional meteorological drought. It has a direct correlation with grassland biomass and vegetation growth [14,15], and is an important index of vegetation to study drought in a growing season.

The China-Mongolia Arid and Semiarid Area (CMASA) is one of the eight major arid regions in the world, and it is also an inland arid region with the highest latitude. Inner Mongolia is located in the transition region between the arid and semi-arid areas in the east of CMASA. Due to the perennial influence of the westerly wind system, atmospheric circulation, and pressure field of Qinghai-Tibet Plateau, temperature rise in the west of Inner Mongolia is significantly higher than that in the inland and surrounding areas of China, and is particularly sensitive to climate change [16,17]. Inner Mongolia is China's main grassland for pasture and agriculture. It is an important ecological barrier to the North of China. For a long time, Inner Mongolia has suffered from frequent regional and local droughts, which have significantly impacted the local economy. The intensification of desertification caused by droughts has become the primary ecological and environmental concern in Inner Mongolia [18]. There are many research activities on long-term drought monitoring in Inner Mongolia: An et al. [19] analyzed the spatiotemporal variation of droughts in Inner Mongolia in the past 60 years; Pei et al. [20] compared the differences and applicability of SPI and SPEI drought indexes at different time scales; Tong et al. [21] used linear regression and wavelet analysis to identify drought changes and drought patterns; however, few studies have quantitatively explained the causes of the droughts. In the past, drought analysis and regional water resource planning were mainly based on linear correlation between factors [22–24]. However, drought is a complex regionalization event. It is generally hard to refine intensity and interaction among various factors in different regions using just the traditional linear regression analysis [25,26]. At the same time, drought is closely related to natural conditions, human activities, and their interactions. However, interactions among these factors have not been well-investigated [27]. Different land cover types, soil conditions, topography, and other factors may cause spatial differentiation of local drought. Geodetector and GWR are statistical models considering spatial nonstationarity and the modeling process is simple but intuitive. A combination of the two can accurately describe the action, path, and intensity of the influencing factors and has a good application prospect [28–30].

In this study, the seasonal SPEI-3 index (SPEI for short) was calculated based on the data at the meteorological stations in Inner Mongolia; the spatiotemporal variation trend of SPEI in the growing season from 2000 to 2018 was obtained using univariate linear trend analysis. The main controlling factors of drought change were identified through Geodetector. The GWR model was used to quantitatively evaluate the effect of various driving factors on SPEI change during the growing season, and to explain the interaction between the main controlling factors for spatial heterogeneity.

2. Materials and Methods

2.1. Study Area

Inner Mongolia is located in the northern border of China, spanning three major regions of northwest, north, and northeast, spreading along a long and narrow belt. The region covers a total area of about 1.183 million km² that accounts for about 12.1% of

China's total area. The region is rich in resources, with grasslands, forests, and arable land per capita ranking first in China. The Greater Khingan Range runs through the east of the study area in the north-south orientation. The Yin Mountains extend east-west in the south. Large deserts such as the Badain Jaran Desert, Tengger Desert, and Mu Us Desert are located in the west. The study area has an average altitude of about 1000 m. The climate in the region varies from arid-semiarid monsoon climate to humid-semi humid climate. It is often affected by cyclones on the Mongolian Plateau with strong wind in spring and by Lake Baikal, the world's largest freshwater lake by volume containing 22–23% of the world's fresh surface water. The climate is often controlled by prevailing westerlies belts or subtropical high-pressure belts, with high temperature and little rain in summer. Annual rainfall showed a decreasing trend from east to west and from north to south [22,31].

2.2. Data Sources and Preprocessing

2.2.1. Meteorological Data

Daily mean air temperature, monthly cumulative precipitation, daily mean wind speed, and daily mean sunshine duration at 110 meteorological stations (Figure 1a) in and around Inner Mongolia from 2000 to 2018 were selected as meteorological data, which were provided by the China Meteorological Data Service Centre (<http://data.cma.cn/>). A homogeneity test of the meteorological data was carried out to fill in unavailable data. A statistical analysis on the mean air temperature ($^{\circ}\text{C}$), accumulated precipitation (mm), mean wind speed ($\text{m}\cdot\text{s}^{-1}$), and mean sunshine duration (h) at stations was performed for the growing seasons from 2001 to 2018. Spatial resolution for ordinary Kriging interpolation was set to $1\text{ km} \times 1\text{ km}$; the geographic reference was set as WGS84/UTM zone 48 $^{\circ}$ N.

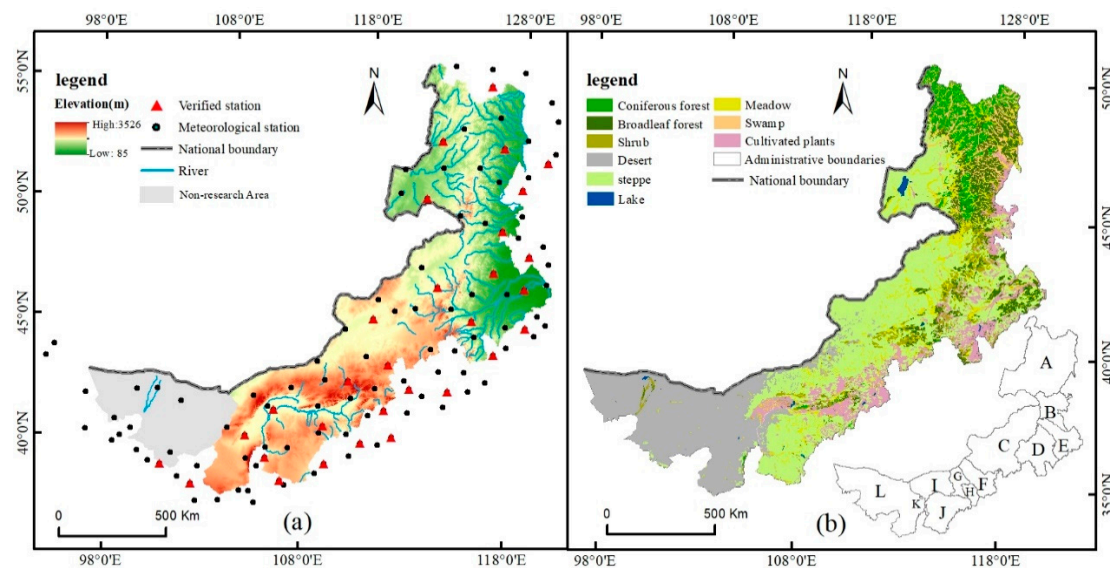


Figure 1. (a) The Digital Elevation Model (DEM) and meteorological station distribution, and (b) the vegetation types in Inner Mongolia (A—Hulunbuir, B—Hinggan League, C—Xilingol League, D—Chifeng, E—Tongliao, F—Ulangab League, G—Baotou, H—Hohhot, I—Bayannur League, J—Erdos, K—Wuhai, L—Alxa League).

2.2.2. DEM Data

DEM (Digital Elevation Model) was the Shuttle Radar Topography Mission (SRTM) data with a resolution of 90 m downloaded from the United States Geological Survey (USGS) data portal (<http://earthexplorer.usgs.gov>). After preprocessing, such as mosaicking and void-filling, the accuracy of the input topographic data had a standard error of 1 m. The DEM data were resampled to $1\text{ km} \times 1\text{ km}$ and slope and aspect were then derived from the DEM data.

2.2.3. Other Data Sets

Population density data was from the population dataset produced by the Landscan Global team (<https://landscan.ornl.gov/>), with a spatial resolution of $0.01^\circ \times 0.01^\circ$ (about 1 km). The data were produced according to the community standard of global population distribution data constructed from multivariable geographic dasymetric modeling and remote sensing image analysis [32]. Land use conversion type can effectively reflect intensity of human activities [33]. It is also an important surface condition for drought research. The land cover data in 2000 and 2018 were from the Resource and Environment Science Data Center of Chinese Academy of Sciences (<http://www.resdc.cn>). The data set was obtained by visual interpretation of Landsat TM/ETM+ images for different periods and was widely used [25]. Land cover was classified into six basic categories: cultivated land, forest, grassland, water area, construction land, and unused land. A land use conversion map from 2000 to 2018 was generated. Soil sediment contents were from the 1:1 million soil type map and the soil profile data was obtained from the second soil survey (<http://www.resdc.cn>). Soil texture was classified according to the content of sand, silt, and clay. The content of particles in different soils was shown as a percentage. Spatial data of main rivers and county stations were derived from the 1:4 million vector database provided by the National Geographic Center of China (<http://ngcc.sbsm.gov.cn>). Distance to Rivers (DTR) and Distance to Cities (DTC) were obtained through buffer zone analysis, and the spatial resolution was set to $1 \text{ km} \times 1 \text{ km}$. The 1:1 million vegetation type data released by the Resource and Environment Science Data Center of the Chinese Academy of Sciences (<http://www.resdc.cn>) were used. The vegetation in Inner Mongolia was reclassified into 8 classes: coniferous forest, broad-leaved forest, shrub, grassland, meadow, swamp, desert, and cultivated vegetation.

2.3. Methods

2.3.1. Calculation of the Standard Precipitation Evapotranspiration Index (SPEI)

The difference between precipitation and potential evapotranspiration (PET), PD , is a key parameter for SPEI calculation. PET was calculated using the Thornthwaite method because fewer meteorological elements are required [9], as follows:

$$PD_i = P_i - PET_i \quad (1)$$

$$PET = 16.0 \times \left(\frac{10T_i}{H} \right)^A \quad (2)$$

$$A = 6.75 \times 10^{-7} H^3 - 7.71 \times 10^{-5} H^2 + 1.79 \times 10^{-2} H + 0.492 \quad (3)$$

where P_i is the monthly precipitation of the i -th month, PET_i the monthly evapotranspiration, A a constant, and H the annual heat index. The log-logistic function based on three parameters (α , β , γ) was used to perform the normal fitting to the time series of PD_i and compute the probability distribution function $F(x)$. The log-logistic probability distribution function is given as below:

$$F(x) = \left[1 + \left(\frac{\alpha}{x - \gamma} \right)^\beta \right]^{-1} \quad (4)$$

where α is the scale parameter, β the shape parameter, and γ the position parameter; all are obtained by the linear-moment method.

The probability distribution function was standardized to obtain the cumulative probability Q (Equation (5)):

$$Q = 1 - F(x) \quad (5)$$

and the SPEI value was then calculated as:

$$SPEI = \begin{cases} w - \frac{a_0 + a_1 w + a_2 w^2}{1 + d_1 w + d_2 w^2 + d_3 w^3}, & w = \sqrt{-2 \ln(Q)} (Q \leq 0.5) \\ -(w - \frac{a_0 + a_1 w + a_2 w^2}{1 + d_1 w + d_2 w^2 + d_3 w^3}), & w = \sqrt{-2 \ln(1 - Q)} (Q \geq 0.5) \end{cases} \quad (6)$$

where the constants $a_0 = 2.515517$, $a_1 = 0.802853$, $a_2 = 0.010328$, $d_1 = 1.432788$, $d_2 = 0.189269$, and $d_3 = 0.001308$. The degree of drought (Table 1) was classified according to the local climate conditions [21,34].

Table 1. Drought classification based on SPEI.

SPEI Value	Drought
>1	Severe wet
(0.5, 1]	Moderate wet
(0, 0.5]	Light wet
(−0.5, 0]	Light drought
(−1, −0.5]	Moderate drought
<−1	Severe drought

2.3.2. Trend Analysis

The univariate linear regression equation (Equation (7)) was used for trend analysis to calculate the variation trend of SPEI during the growing seasons from 2000 to 2018:

$$\theta_{slope} = \frac{n \times \sum_{i=1}^n (i \times SPEI_i) - \sum_{i=1}^n i \sum_{i=1}^n SPEI_i}{n \times \sum_{i=1}^n i^2 - \left(\sum_{i=1}^n i\right)^2} \quad (7)$$

where n ($n = 19$) is the length of time series and θ_{slope} is the slope in the linear regression equation. $\theta_{slope} > 0$ indicates that the drought trend is reduced; otherwise, the drought is aggravated. The variation trend of SPEI was divided into five levels based on the standard deviation (STD), i.e., significant degradation ($\theta_{slope} < -STD$), slight degradation ($-STD < \theta_{slope} < -0.5STD$), substantially unchanged ($-0.5STD < \theta_{slope} < 0.5STD$), slight improvement ($0.5STD < \theta_{slope} < STD$), and significant improvement ($\theta_{slope} > STD$).

2.3.3. Geodetector

Geodetector is a spatial statistical model based on spatial autocorrelation theory to reveal the spatial differentiation of geographic elements and their driving factors [30]. We mainly used the factor detector, ecological detector, and interactive detector within the model. The factor detector quantifies the contribution of influencing factors to dependent variables, and it is calculated as follows:

$$q = 1 - \frac{SSW}{SST} \quad (8)$$

$$SSW = \sum_{h=1}^l N_h \sigma_h^2, SST = N \sigma^2 \quad (9)$$

where SSW is the sum of factor variances over all layers and SST is the total sum of variance, where $h = 1, \dots, l$ is the number of strata of the dependent variable or independent variable; N_h and N are the number of units in class h and the whole region, respectively; and σ_h^2 and σ^2 are the variances of the dependent variable for the units in class h and the whole region, respectively. The larger the q -value is, the stronger the explanatory power of the factor to the drought phenomenon. The effective range of q is [0, 1].

The ecological detector uses an F test to measure the significant difference of the impact of different influencing factors on the spatial distribution of drought. The F value is determined as follows:

$$F = \frac{N_{n=1}(N_{n=2} - 1)\sigma_{n-1}^2}{N_{n=2}(N_{n=1} - 1)\sigma_{n-2}^2} \quad (10)$$

where $N_{n=1}$ and $N_{n=2}$ refer to the sample size of two random factors, and F reflects the significance level.

The interaction detector was used to identify whether two driving factors, x_1 and x_2 , increase or decrease the explanatory power of the drought index SPEI when they work together (Table 2).

Table 2. Independent variable interaction type.

Judgement Condition	Interaction
$q(x_1 \cap x_2) < \text{Min}(q(x_1), q(x_2))$	Non-linearly weaken
$\text{Min}(q(x_1), q(x_2)) < q(x_1 \cap x_2) < \text{Max}(q(x_1), q(x_2))$	Non-linearly weaken by one factor
$q(x_1 \cap x_2) > \text{Max}(q(x_1), q(x_2))$	Mutually enhanced
$q(x_1 \cap x_2) = q(x_1) + q(x_2)$	Independent effect
$q(x_1 \cap x_2) > q(x_1) + q(x_2)$	Non-linearly enhanced

In addition to the influences of meteorological variables, droughts are also affected by other factors including geographic location, topography, soil, land cover type, human activities, etc. Land cover type affects runoff, infiltration, and evapotranspiration of surface water through water absorption [35]. We selected 12 potential drought driving factors as follows: Mean Air Temperature (MAT), Mean Precipitation (MP), Mean Wind Speed (MWS), and Mean Sunshine Duration (MSD) during the growing season, representing the meteorological conditions; Percent of Sand (POS) in soil, representing soil texture; elevation, slope, and slope aspect, representing topographic conditions; Distance to rivers (DTR), representing potential water availability; Distance to Prefecture Cities (DTC), Land-Use and Land-Cover Change (LUCC), and Average of population Density (AOPD), representing human factors that can transform and regulate the local environment [36]. These factors are easy to be quantified [25,37,38]. Since Geodetector can only handle discrete variables, the 12 variables need to be discretized individually. The LUCC factors were divided into 36 grades according to the land use type conversion maps from 2000 to 2018, the slope and aspect were divided into 9 grades, and each of the other 10 factors was divided into 6 grades by the Jenks Natural Breaks Classification Method (Figure 2).

2.3.4. The GWR Model

The GWR model is an extension of the ordinary linear regression analysis method [39], which can effectively estimate the data with spatial autocorrelation and reflect the spatial heterogeneity of parameters in different regions. The multi-variate linear regression equation is given by:

$$y_i = \beta_0(u_i, v_i) + \sum_{j=1}^n \beta_j(u_i, v_i)x_{ij} + \varepsilon_i \quad (11)$$

where β_0 represents the intercept; (u_i, v_i) represent the coordinates of the i -th sampling point; $\beta_j(u_i, v_i)$ the j -th regression parameter on the i -th sampling point, which has geographic significance; $x_{i1}, x_{i2}, x_{i3}, \dots, x_{in}$ are n regression variables at this point; and ε represents random error. Finally, the revised Akaike Information Criterion (AIC) was compared with the ordinary least squares (OLS) results. AIC is defined as:

$$AIC = -2\ln L(\hat{e}_L, y) + 2c \quad (12)$$

where y represents the sample set of the fitting value of the dependent variable SPEI, $L(\hat{e}_L, y)$ is the likelihood function, \hat{e}_L is the maximum likelihood estimate of e_L , and c is the number of unknown parameters. The smaller the AIC is, the higher the fitting degree will be.

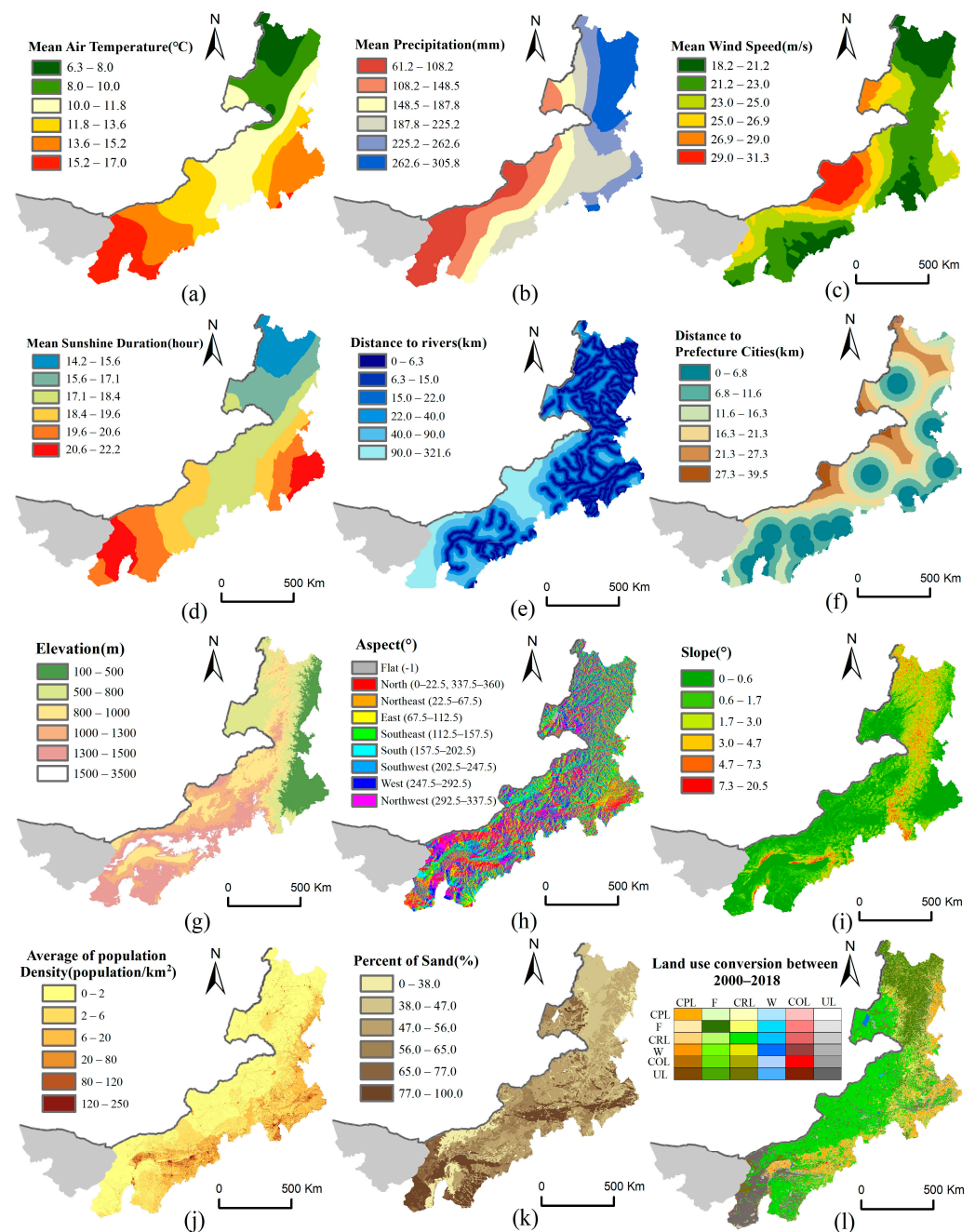


Figure 2. Factor grading (MAT(a), MP (b), MWS (c), MSD (d), DTR (e), DTC (f), Elevation (g), Aspect (h), Slope (i), AOPD (j), POS (k), LUCC (l) (CPL: CropLand; F: Frost; CRL: Crass Land; W: Water Area; COL: Construction Land; UL: Unused Land)).

3. Results and Analysis

3.1. Spatiotemporal Variation Characteristics of SPEI

The result of SPEI interpolation cross-validation shows a Pearson correlation coefficient of $r = 0.85$ and root-mean-square error $RMSE = 1.15$, indicating that the SPEI interpolation result has high accuracy. The statistical results of SPEI in the study area over the years show that (Table 3) the average annual SPEI of the growing season in Inner Mongolia from 2000 to 2018 is -0.03 , representing a mild drought. The area in mild drought during the growing season reached $532,600 \text{ km}^2$, accounting for 52.39% of the total study area. The area in mild drought was the largest in 2000, accounting for 99.60% of the total, followed by 2001 and 2017, and that in 2012 was the smallest, accounting for only 6.01% of the total. Among the various types of droughts, the average annual area of mild drought accounted

for about 74.34%, the highest proportion. The largest areas of moderate drought and severe drought occurred in 2000 and 2005, accounting for 73.10% and 36.17%, respectively.

Table 3. Change of drought area and proportion of various types of drought area in the study area from 2000 to 2018.

Year	Drought Area (Ten Thousand Km ²)	Percentage of Study Area	Percentage of Light Drought	Percentage of Moderate Drought	Percentage of Severe Drought	SPEI
2000	101.25	99.6%	23.28%	73.10%	3.62%	−0.62
2001	96.49	94.98%	20.44%	68.36%	11.21%	−0.68
2002	55.60	54.79%	73.00%	20.60%	6.39%	−0.01
2003	7.74	7.62%	100%	0	0	0.66
2004	51.40	50.59%	60.17%	39.82%	0.02%	0.03
2005	69.74	68.65%	33.45%	30.38%	36.17%	−0.43
2006	65.55	64.52%	98.63%	1.37%	0	−0.06
2007	84.12	82.80%	25.98%	40.67%	33.35%	−0.59
2008	16.74	16.48%	96.58%	3.42%	0	0.29
2009	73.59	72.43%	35.96%	53.26%	10.78%	−0.39
2010	66.59	65.54%	99.68%	0.32%	0	−0.03
2011	62.57	61.59%	69.74%	30.26%	0	−0.16
2012	6.11	6.01%	90.94%	9.06%	0	0.77
2013	29.32	28.86%	52.46%	26.51%	21.03%	0.51
2014	11.19	11.02%	100%	0	0	0.36
2015	17.87	17.59%	99.99%	0.01%	0	0.37
2016	34.37	33.80%	100%	0	0	0.19
2017	88.27	86.88%	28.08%	49.06%	22.86%	−0.61
2018	73.46	72.31%	68.36%	31.64%	0	−0.21
Annual average	53.26	52.39%	74.34%	18.89%	6.7%	0.03

The study area has high elevation in the west and low in the east (Figure 1a), and high in the south and low in the north. The spatial distribution of SPEI shows an increasing pattern from west to east with a rate of change of 0.008/degree and an increase of 0.01/degree from south to north (Figure 3). SPEI is highly sensitive to elevation gradients. Areas with high SPEI were mainly distributed in the 40~52°N area below 800 m in elevation, including Hinggan League, Hulunbuir City, Bairin Left Banner of Chifeng City, and other areas (Figure 1b); low SPEI appeared in areas with elevation between 1100 m~1400 m, in longitude between 105~115°E, and latitude between 40~45°N, mainly including Bayannur City, Baotou City, Ulanqab City, and West Ujimqin Banner of Xilingol League. In the Banner area, land covers are mainly grasslands, meadows, and deserts (Figure 1b).

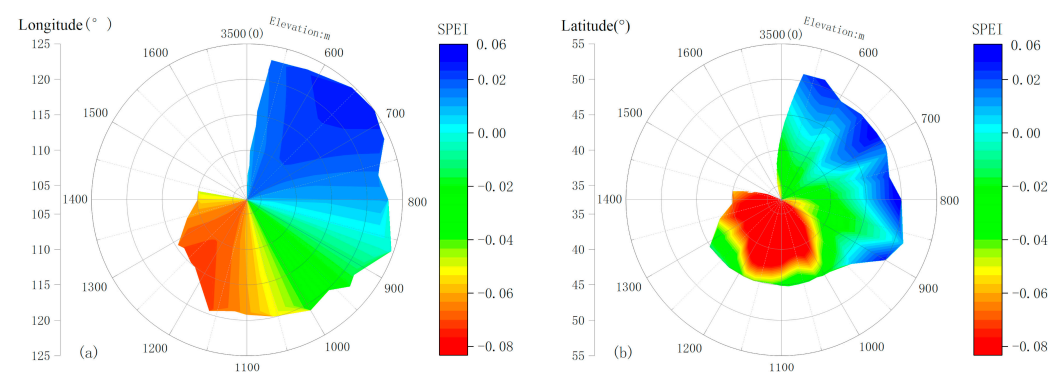


Figure 3. Spatial distribution of multi-year mean values of SPEI during the growing season in the study area from 2000 to 2018. (a) Longitude and elevation statistics. (b) Latitude and elevation statistics.

Trend analysis results show that (Figure 4a) there are significant differences in SPEI changes between the east and west of the study area. SPEI decreased with time significantly at a rate of $-0.40 \sim -0.25 \cdot (10a^{-1})$ in the west including Alxa Left Banner in Alxa League, Dorbod Banner in Ulanqab City, Darhan Muminggan United Banner in Baotou City, and Wuhai City, while SPEI increased significantly with time at a rate of change of $0.25 \sim 0.75 \cdot (10a^{-1})$ in Hulunbuir City, Hinggan League, Tongliao City, and the eastern part of Xilingol League. On the whole, the area with elevated SPEI was about 819,190 km², accounting for 79.70% of the study area. The land cover in the study area was relatively high in grassland, desert, and cultivated vegetation, reaching 43.68%, 11.94%, and 11.07%, respectively. The area of marsh was the smallest, accounting for only 3.69%. There are significant differences in the spatial distribution of vegetation (Figure 4b). The results of the SPEI variation trend in different land cover types showed that the area with a significantly higher SPEI (SPEI > STD) accounted for about 44.10% of the study area. The increasing trends of SPEI in swamp, coniferous forest, and broad-leaved forest were the most obvious, accounting for more than 85%. These land covers were located in a high-latitude, low-altitude forest area. The area has a large amount of precipitation, abundant water resource, and a low probability of drought. About 93.12% of the area where SPEI dropped significantly was located in the desert, accounting for about 61.53% of the total desert area. In the past 20 years, the mean annual precipitation in the desert areas of Inner Mongolia was less than 150 mm. Under the high-temperature and high-evaporation climatic conditions, water loss became severe and terrestrial carbon productivity was restricted, leading to an increased risk of drought [40].

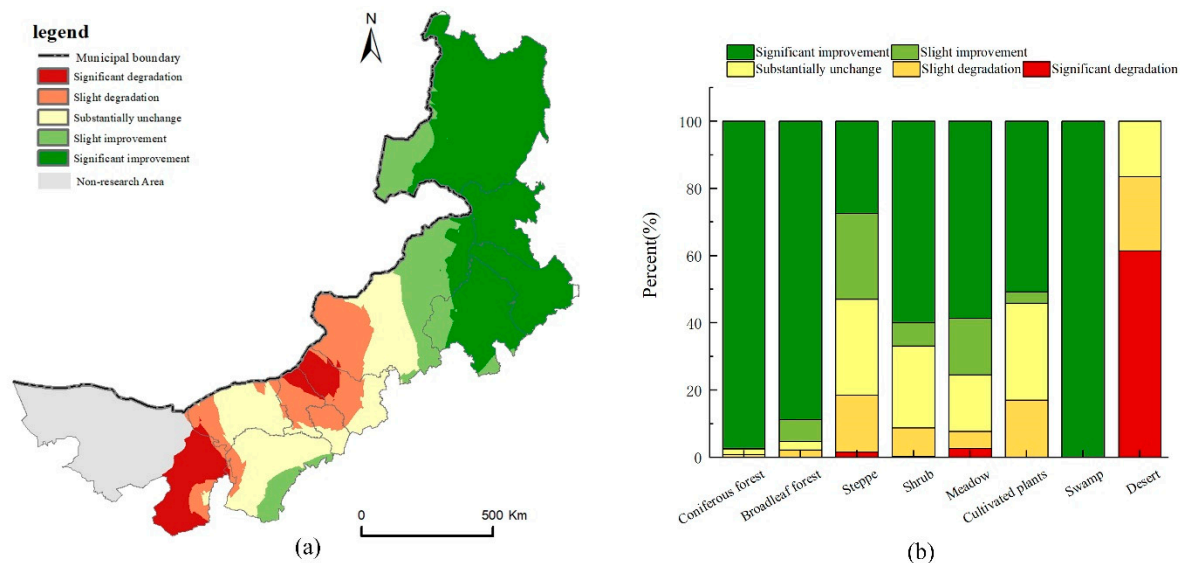


Figure 4. (a) The distribution of SPEI trend and (b) area percent in different land cover type.

3.2. Identification of Main Control Factors

The factor detection and ecological detection show that (Table 4) precipitation was the most explanatory factor ($q = 0.73$). From the q -values (Table 4), we can see the top four impact factors in decreasing order were MP > Elevation > MAT > DTR, and all passed the significance test ($p < 0.05$). Slope, aspect, LUCC, AOPD, and DTC have lower explanatory power for drought.

Table 4. q statistics and ecological detector.

Factor	Tag	p Value	q -Value	Rank
MAT	X_1	0.05	0.43	3
MP	X_2	0.05	0.73	1
MWS	X_3	0.05	0.13	
MSD	X_4	0.05	0.22	
DTR	X_5	0.05	0.42	4
DTC	X_6	0.05	0.03	
Elevation	X_7	0.05	0.53	2
Aspect	X_8	>0.1	0.01	
Slope	X_9	0.05	0.11	
AOPD	X_{10}	>0.1	0.06	
POS	X_{11}	0.05	0.23	
LUCC	X_{12}	0.05	0.26	

SPEI rates of change (θ_{slope}) versus factor level for various factors were shown in Figure 5. We can see that θ_{slope} shows a decreasing trend (Figure 5a), with increasing factor level for factors MAT (X_1), MSD (X_4), DTR (X_5), and elevation (X_7). The elevation factor has the greatest influence on θ_{slope} when the factor level is low (≤ 2), while factors MAT and MSD have a larger impact at a high factor level (> 4). The elevation increases from the first level (100~500 m) to the fifth level (1500~3500 m), and the θ_{slope} decreases from $0.58 \cdot (10 \text{ yr}^{-1})$ to $-0.02 \cdot (10 \text{ yr}^{-1})$. Compared with other factors, the influence of DTR on θ_{slope} is approximately linear, and θ_{slope} drops to the lowest value ($0.08 \cdot (10 \text{ yr}^{-1})$) in the DTR interval of 90~321.6 km. On the contrary, θ_{slope} shows an increasing trend (Figure 5c) with the increasing factor level of MP (X_2), MWS (X_3), and Slope (X_9). Precipitation has the greatest impact on θ_{slope} . The amount of precipitation increases from level 1 (61.2~108.2 mm) to level 5 (262.6~305.8 mm), and θ_{slope} rises from $-0.075 \cdot (10 \text{ yr}^{-1})$ to $0.53 \cdot (10 \text{ yr}^{-1})$. The relationship between θ_{slope} and any of the following factors, DTC (X_6), aspect (X_8), AOPD (X_{10}), and POS (X_{11}), does not show a significant linear trend (Figure 5b). When POS is at the second level (38~47%), θ_{slope} reaches a peak value. This may imply that appropriate amount of sand is conducive to the respiration of plant roots, retaining soil moisture, and transportation of nutrients. However, a percentage of sand that is too high can easily cause surface degradation, soil moisture loss, and soil erosion. DTC, aspect, and AOPD have much smaller variation ranges of θ_{slope} , which indicates that these factors have little influence on the change of SPEI rate. SPEI over most land cover types (X_{12}) increased from 2000 to 2018, and SPEI decreased over only two land covers, in which cases water area was converted to construction area and unused land (Figure 5d). The θ_{slope} of the two land covers was $-0.09 \cdot (10 \text{ yr}^{-1})$ and $-0.03 \cdot (10 \text{ yr}^{-1})$, accounting for 0.1% and 11.5% of the study area, respectively. Among all land conversion types, the SPEI of unaltered forest land increased at the fastest rate $0.51 \cdot (10 \text{ yr}^{-1})$.

Overall, the factors with strong explanatory power in the factor detector have a larger fluctuation range of θ_{slope} . The θ_{slope} values of factors such as MP, elevation, MAT, and DTR are in four ranges of $-0.07 \sim 0.55$, $-0.02 \sim 0.58$, $-0.04 \sim 0.53$, and $-0.09 \sim 0.44 \cdot (10 \text{ yr}^{-1})$, respectively. The change range of SPEI rate influenced by natural factors, such as meteorology and topography in the study area, was larger than that influenced by human factors.

The ranking of the influence by interacting pair of factors was given in Table 5. Only the precipitation \cap DTC ($X_2 \cap X_7$) and wind speed \cap elevation ($X_1 \cap X_2$) pairs of the first 15 interacting pairs showed nonlinear enhancement; the others were dual-factor enhancement. Among them, the influence by the interaction between precipitation and elevation is the strongest, with a q -value of 0.870, followed by that between temperature and precipitation; the interaction between wind speed and elevation has the lowest explanatory power, with a q -value of 0.686. As expected, precipitation is an important source of water and a crucial driving factor in the process of drought changes. The difference in precipitation between the east and west of Inner Mongolia contributes mainly to the spatial

differentiation of drought condition. Elevation also has a strong explanatory power for drought. It is an important topographical factor for driving drought in Inner Mongolia, and it is also an important factor in combining other factors to form a drought spatial pattern.

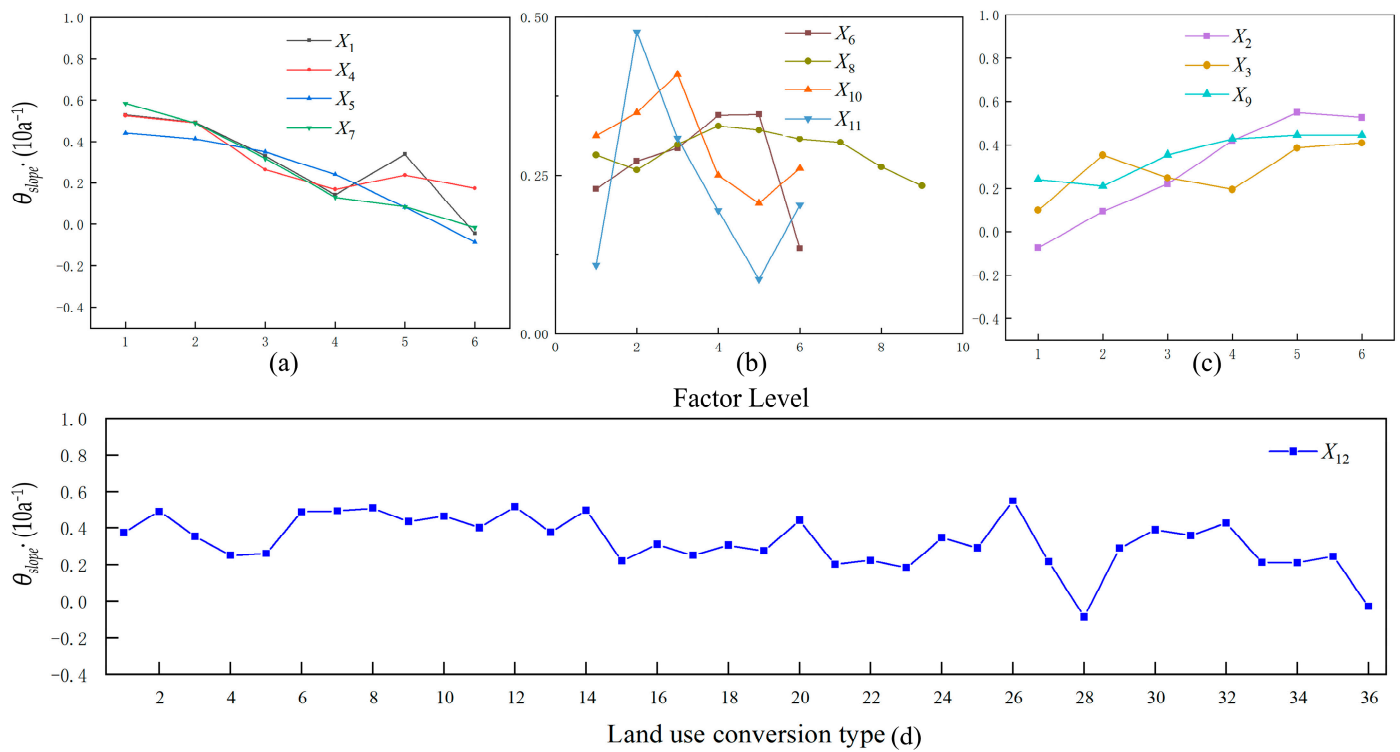


Figure 5. SPEI’s variation trend with the influence of (a) MAT (X_1), MSD (X_4), DTR (X_5), Elevation (X_7); (b) DTC (X_6), Aspect (X_8), AOPD (X_{10}), POS (X_{11}); (c) MP (X_2), MWS (X_3), Slope (X_9); (d) LUCC (X_{12}) with their levels. The meanings of the land cover and land use codes for land use conversion types can be found in Figure 2.

Table 5. Influence of the interacting pairs of factors.

$q = A \cap B$	Results Comparison	Interaction Type	Rank
$X_1 \cap X_2 = 0.852$	$X_1 + X_2 > \text{Max}(X_1, X_2)$	Double-factor Enhance	2
$X_1 \cap X_7 = 0.753$	$X_1 + X_7 > \text{Max}(X_1, X_7)$	Double-factor Enhance	8
$X_2 \cap X_3 = 0.846$	$X_2 + X_3 > \text{Max}(X_2, X_3)$	Double-factor Enhance	3
$X_2 \cap X_4 = 0.836$	$X_2 + X_4 > \text{Max}(X_2, X_4)$	Double-factor Enhance	4
$X_2 \cap X_5 = 0.742$	$X_2 + X_5 > \text{Max}(X_2, X_5)$	Double-factor Enhance	11
$X_2 \cap X_6 = 0.770$	$X_2 + X_6 < X_2 \cap X_6$	Nonlinear Enhance	5
$X_2 \cap X_7 = 0.870$	$X_2 + X_7 > \text{Max}(X_2, X_7)$	Double-factor Enhance	1
$X_2 \cap X_9 = 0.745$	$X_2 + X_9 > \text{Max}(X_2, X_9)$	Double-factor Enhance	10
$X_2 \cap X_{10} = 0.756$	$X_2 + X_{10} > \text{Max}(X_2, X_{10})$	Double-factor Enhance	7
$X_2 \cap X_{11} = 0.751$	$X_2 + X_{11} > \text{Max}(X_2, X_{11})$	Double-factor Enhance	9
$X_2 \cap X_{12} = 0.762$	$X_2 + X_{12} > \text{Max}(X_2, X_{12})$	Double-factor Enhance	6
$X_3 \cap X_7 = 0.686$	$X_3 + X_7 < X_3 \cap X_7$	Nonlinear Enhance	15
$X_4 \cap X_7 = 0.737$	$X_4 + X_7 > \text{Max}(X_4, X_7)$	Double-factor Enhance	12
$X_5 \cap X_7 = 0.695$	$X_5 + X_7 > \text{Max}(X_5, X_7)$	Double-factor Enhance	14
$X_7 \cap X_{10} = 0.703$	$X_7 + X_{10} > \text{Max}(X_7, X_{10})$	Double-factor Enhance	13

Note: Only the first 15 combinations are ranked.

3.3. Spatial Difference of Main Control Factors

The GWR model was used to perform spatial regression analysis on the four main controlling factors, i.e., MAT, MP, Elevation, and DTR, and local adjusted R^2 and Akaike Information Criterion (AIC) as the evaluation indexes of the model fitting. Results show that the adjusted R^2 of the GWR model is 0.88, and the AIC value is -540.58 . The action

direction of the factor is reflected by the sign of the coefficient of the fitting equation. A negative coefficient in an area and the absolute value of the coefficient indicate that the area is drought-stricken and the strength of the driving effect, respectively.

The effects of the two meteorological factors, i.e., temperature and precipitation, have significant spatial differences. The overall fluctuation ranges of the two are relatively large, and the regression coefficient intervals are $(-1.20, 0.60)$ and $(-1.4, 0.55)$, respectively. The area in drought driven by temperature accounted for about 70.2%, of which the areas with strong temperature driving $(-0.6\sim-1.20)$ were mainly located in Alxa Left Banner of Alxa League, Wuhai City, Hanggin Banner and Otog Banner of Ordos City, Urad Rear Banner of Bayannur City, and parts of Xilingol League (Figure 6a). Due to the large temperature difference between the east and west of the study area (up to $12.7\text{ }^{\circ}\text{C}$), the surface vegetation in the western hot area had strong transpiration and respiration, and the dry matter consumption and soil water loss were larger, which further expanded the arid area [41,42]. The difference of the driving results between precipitation and temperature factors is mainly in the semi-arid grasslands (Figure 6b), such as Xilinhot City, West Ujimqin Banner and East Ujimqin Banner in Xilingol League. The average precipitation in the growing season in this region was greater than 150 mm, which was enough for the growth of vegetation such as grassland, shrubs, and other vegetation [43].

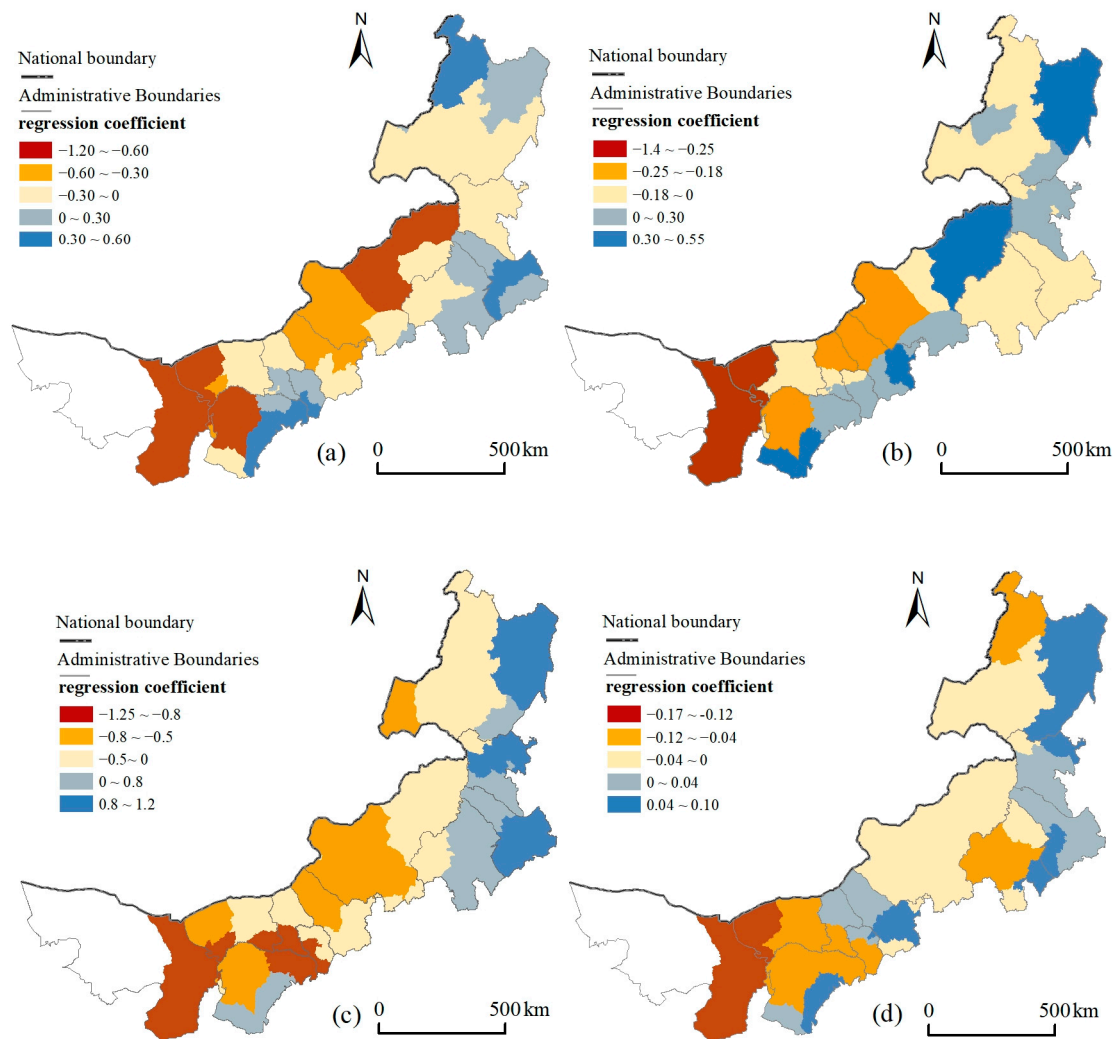


Figure 6. Distribution of the regression coefficient of SPEI with (a) MAT, (b) MP, (c) Elevation, and (d) DTR.

The influence of elevation mainly reflects the effect of the terrain. The GWR regression coefficient interval is $(-1.25, 1.2)$, with the Great Khingan Range-Yin Mountains-Helan Mountains range as the boundary, and the SPEI driving coefficients on both sides are obviously different (Figure 6c). The central and western regions of Inner Mongolia (Alxa Left Banner, Dalate Banner, Zhungeer Banner, etc.) dominated by the Mongolian Plateau are generally higher than 1000 m in elevation, which has a significant effect on drought. The average GWR coefficient is -0.75 . The eastern foothills of the Great Khingan Range-Yin Mountains and the southern foothills of Helan Mountains have lower average elevations, ranging from 100 to 500 m, and the average GWR coefficient is 0.5 . The DTR factor reflects the water conservation within the basin, and the range of coefficient is the smallest $(-0.17, 0.12)$. Due to low water conservation in Alxa League, Wuhai City, Ordos City, and Erguna in Hulunbuir City, the impact by DTR is shown in Figure 6d: the drought mitigation area driven by DTR is mainly located at the tributary of the Yellow River in Ordos City in the southwest of Inner Mongolia, Tabu River in Ulanqab City, and Dahei River (River inflow area), and the areas where Liaohe River, Songhua River, Nenjiang River, and other rivers adjacent to the Northeast Plain flow through.

4. Discussion

4.1. Driving Analysis of Drought in the Inner Mongolia

Drought is mainly caused by the imbalance of regional precipitation and evapotranspiration. We found that the change rate of SPEI during the growing season in Inner Mongolia from 2000 to 2018 ranged from -0.4 to $0.75 \cdot (10 \text{ yr}^{-1})$, and the area with decreasing SPEI accounted for 20.3% of the total area. The areas where the SPEI increased significantly (θ_{slope} is between 0.25 and $0.75 \cdot (10 \text{ yr}^{-1})$) are mainly located in Hulunbuir City, Hinggan League, and Tongliao City. The distribution characteristics of SPEI shown in this study are similar to the results of previous drought monitoring based on long-term series [19,20]. The differences are mainly manifested in the areas such as Hinggan League and Tongliao City, where drought changes increased significantly. Around 2000, the SPEI time series of the Mongolian Plateau showed a significant turning point from increasing to decreasing [34,44]. The results of the Geodetector modeling showed that the SPEI change was driven by four main controlling factors: air temperature, precipitation, DTR, and elevation (Table 4) during the growing season in the study area. Precipitation is a direct factor in drought ($q = 0.73$). Relevant studies have shown that in arid and semi-arid areas, vegetation growth and ecosystem health status depend directly on atmospheric precipitation [45]. The interaction detection results show that the joint effect of precipitation and elevation has the most explanatory power ($q = 0.87$). Conclusions about attribution analysis of drought agreed with a previous study [36]. However, we considered the special climatic background of Inner Mongolia in this study of meteorological drought. The impact of elevation reflects the influence of topography on mass and energy transportation and distribution of temperature and water availability that affect regional ecosystems through altering vegetation species and distribution and the formation and evolution of regional climate [46]. According to the drought trend (Figure 4a) and the spatial distribution of the regression coefficient of SPEI with GWR model factors (Figure 6), it was found that significantly reduced SPEI at a rate of $-0.40 \sim -0.25 \cdot (10 \text{ yr}^{-1})$ occurred in Alxa Left Banner in Alxa League, Dorbod Banner chain Ulanqab City, Darhan Muminggan United Banner in Baotou City, and Wuhai City in the western part of the study area. The drought in Alxa League and Wuhai City was caused by a synergy of hot air temperature, lack of precipitation, high elevation, and high DTR, while the drought in Ulanqab City and Baotou City was mainly caused by hot air temperature, lack of precipitation, and high elevation.

4.2. Variation of Explanatory Power of Factors in Different Elevations

Due to the large and high terrain environment of the Qinghai-Tibet Plateau in the region of the China-Mongolia Arid and Semiarid Area (CMASA), the lack of water vapor transported over the central and western Inner Mongolia has resulted in scarce precip-

itation [47]. The central and western part of the study area is dominated by plateaus and mountains. Due to the barrier and uplifting effects of the Great Khingan Range-Yin Mountains-Helan Mountains on water vapor, the eastern and southern piedmont of the mountains are the East Asian monsoon zone (elevation is about 150~500 m) and the west piedmont of the mountains is the non-monsoon zone (the elevation is generally higher than 1000 m).

As an important terrain factor, elevation has a significant impact on the spatial correlation of factors. We found an interesting pattern to speculate the relative importance of environmental and anthropogenic factors in our study area by elevation gradients. As the statistical results of q -values of various factors in different elevation intervals (Figure 7a), in the 100–500 m elevation interval, the average precipitation (X_1) in the growing season is 261.5 mm, and the q -value is the smallest. When the precipitation reaches a certain level, the impact of precipitation on SPEI decreases [48]. For the forest area, the ecological water storage is sufficient and the correlation between SPEI and sunshine duration (X_4) is stronger. In the elevation range of 800~1000 m, the q -values of factors such as air temperature (X_1), precipitation (X_2), sunshine duration (X_4), slope (X_9), POS (X_{11}), and LUCC (X_{12}) increased significantly, indicating that the change in SPEI was mainly affected by natural factors and some human activities. When the elevation increases to 1000~1300 m, the q -values of POS (X_{11}) and LUCC (X_{12}) reach the maximum of 0.38 and 0.42, respectively, and the q -values of other factors show a downward trend. In the area above 1300 m in elevation, the explanatory power of all factors decreases significantly with increasing elevation.

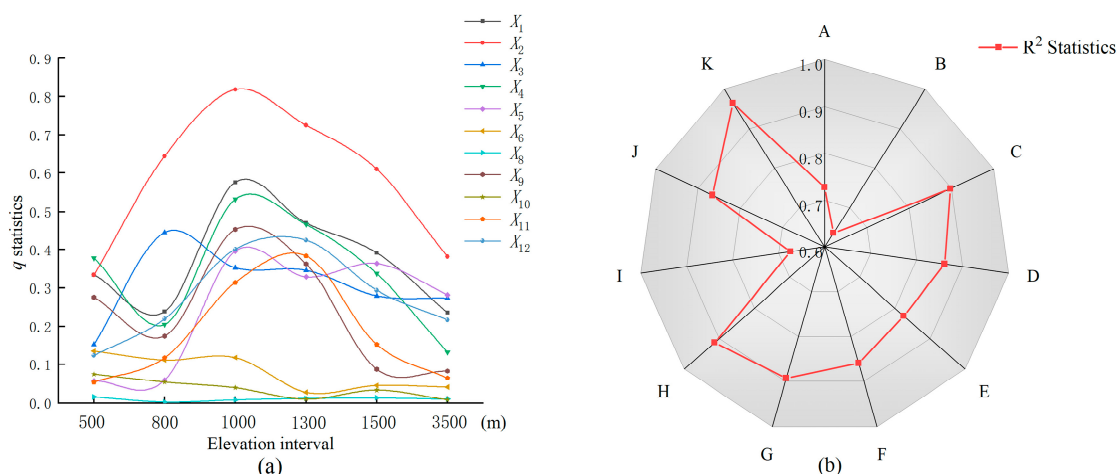


Figure 7. The change in q statistics of influencing factors on SPEI along the gradient of Elevation (a) and R^2 statistics of prefecture cities (b).

It is worth mentioning that the conversion of land use types is an important influencing factor reflecting human activities, as well as an important explanatory factor for drought changes (Table 3). Between 2000 and 2018, in the 800~1300 m elevation interval, SPEI was significantly enhanced by the land use conversion. According to statistics, the land use types that account for the largest area in this elevation interval are unaltered woodland and unaltered grassland (Table 6), which account for 48.3% and 15.5% of the total area of the region, respectively. The growth rates of SPEI are $0.52 \cdot (10 \text{ yr}^{-1})$ and $0.018 \cdot (10 \text{ yr}^{-1})$, respectively, indicating that the series of ecological restoration projects such as “closing hills for afforestation and reforestation, retiring grazing and raising grass” implemented by the Chinese government in Inner Mongolia since 2000 have played an important role [49]. In addition, in the conversion of land use from unused land to grassland and from farmland to grassland, SPEI increased by 0.24 and 0.58, respectively, which alleviated the drought conditions in the area to a large extent (Figure 5d). The SPEI of the unchanged farmland increased by 0.57, and the SPEI growth rate was $0.019 \cdot (10 \text{ yr}^{-1})$. This may be related to improvement in irrigation. Modern irrigation technology has improved the utilization

rate of water resources and increased the field water holding capacity [50]. At the same time, grassland degradation caused by overgrazing and long-term abandonment of land aggravated the degree of drought [51,52]. For example, the grassland in the 800–1300 m elevation range was converted to unused land; as a result, the SPEI decreased by 0.42, while the SPEI of unaltered unused land decreased by 0.21.

Table 6. The area of specific land use conversion in 800–1300 m.

2000/2018 Unit: Km ²	Croplands	Forests	Grasslands	Water Areas	Construction Lands	Unused Lands
Croplands	14,143.289 (3.5)	948.394 (0.2)	7180.634 (1.8)	464.368 (0.1)	1530.627 (0.4)	1758.953 (0.4)
Forests	1357.162 (0.3)	61,982.534 (15.5)	17,312.724 (4.3)	0	0	811.536 (0.2)
Grasslands	5566.708 (1.4)	5677.182 (1.4)	193,072.543 (48.3)	1278.544 (0.3)	735.711 (0.2)	13,980.681 (3.5)
Water areas	477.401 (0.1)	0	952.564 (0.2)	2410.992 (0.6)	0	986.008 (0.2)
Construction lands	1372.649 (0.3)	159.97 (0.1)	1920.498 (0.5)	0	1092.653 (0.3)	492.902 (0.1)
Unused lands	626.973 (0.2)	3200.702 (0.8)	14,295.369 (3.6)	871.862 (0.2)	117.173 (0.1)	43,698.632 (10.9)

Note: The numbers in parentheses are the percentage of specific land use conversion to the total area (%).

4.3. Advantages and Limitations of GWR

The adjusted R^2 value from the GWR model is 0.88, and the AIC value is -540.58 . Compared with the OLS model ($R^2 = 0.54$, $AIC = -504.22$), the AIC value is reduced by 36.36 and the degree of fit is higher, but there are regional differences. The regional statistics of R^2 shows that (Figure 7b) the largest value occurred in Wuhai City, Inner Mongolia (K) $R^2 = 0.96$, followed by Hohhot City (H) $R^2 = 0.92$, and the two prefecture-level cities with the smallest R^2 were Hinggan League (B) and Bayan. In Bayannur City (I), R^2 is 0.64 and 0.67, respectively. The difference in the accuracy of regional fitting may be related to the influence of elevation changes on the distribution of other factors in the large east-west span of the study area. Areas with small R^2 (A, B, I) have an average elevation of less than 800 m, and the average single factor q -value is 0.17. The average elevation of Wuhai City (K) and Hohhot City (H) are 1193 m and 1379 m, respectively, and the average q -value is 0.32 and 0.28, respectively. On the other hand, the area of each city is quite different, so is the statistical sample size, and the collinearity of the factors within the region may be another reason for the low fit in Hinggan League (B) and Bayannur City (I) [11,53,54].

4.4. Future Directions

Compared with traditional statistical models, we quantified the non-linear responses of independent variables and their interactions to SPEI change, without input of complex parameters. Further research may include: (1) using long-term SPEI data and more accurate PET calculation methods, such as the Penman and Hargreaves–Samani formula to produce more generalizable drought-driven results; (2) refining the spatial scale both horizontally and vertically, especially in eastern Inner Mongolia and western Mongolia, to generate results at higher resolutions.

5. Conclusions

Based on the multi-source data at the 110 meteorological stations, DEM, and vegetation types in Inner Mongolia and its surrounding areas, this study investigated the spatiotemporal variation of SPEI during the growing season in Inner Mongolia from 2000 to 2018. Through the introduction of time rate of change in SPEI, we used Geodetector and GWR models to screen the main controlling factors and then effectively quantified the impact of the factors on drought changes and the results are of great significance for

drought-driven research. We made the following conclusions. (1) The SPEI in the growing season from 2000 to 2018 in Inner Mongolia showed a spatial variation pattern from dry west to wet east. The area with light drought accounts for the largest proportion in the whole region. (2) The inter-annual variation of SPEI shows an upward trend and the area of elevated SPEI accounted for 79.70% of the study area. These results indicate that the drought condition became alleviated with time during the growing season in Inner Mongolia. (3) The drought changes in Inner Mongolia were generally controlled by natural factors, with nonlinear interaction between factors enhancing drought impact. The aggravated drought in the central and western regions of the study area, such as Alxa League, Ulanqab City, Baotou City, and Wuhai City, were mainly driven by a synergy of hot air temperature, scarce precipitation, and high elevation, with significant impact from soil and LUCC at an elevation of 800–1300 m. The results from this study should be helpful for decision-making and management of regional water resources.

Author Contributions: Conceptualization, B.J.; formal analysis, Y.Q.; funding acquisition, G.Y.; methodology, M.Z.; software, M.L.; supervision, T.Z. and G.Y.; validation, X.Z.; visualization, Y.Q.; writing—original draft, B.J.; writing—review & editing, Y.Q., X.Z. and T.Z. All authors have read and agreed to the published version of the manuscript.

Funding: This research was funded by the National Natural Science Foundation of China (41801099), the second Tibetan Plateau Scientific Expedition and Research Program (2019QZKK0307), and the Key Research and Development Program of Sichuan (2022YFS0491).

Data Availability Statement: The meteorological data are available at <http://data.cma.cn>, accessed on 12 June 2022. The DEM are available at <https://earthexplorer.usgs.gov/>, accessed on 11 June 2022. The Population density data are available at <https://landscan.ornl.gov/>, accessed on 12 June 2022. The vegetation types data, land cover data, soil texture are available at <https://www.resdc.cn/>, accessed on 12 June 2022. Main rivers and county stations are available at <http://ngcc.sbsm.gov.cn>, accessed on 13 June 2022.

Conflicts of Interest: The authors declare no conflict of interest.

References

- Mishra, A.K.; Singh, V.P. A review of drought concepts. *J. Hydrol.* **2010**, *391*, 202–216. [[CrossRef](#)]
- Liu, D.; Ogaya, R.; Barbeta, A.; Yang, X.; Peñuelas, J. Contrasting impacts of continuous moderate drought and episodic severe droughts on the aboveground-biomass increment and litterfall of three coexisting Mediterranean woody species. *Glob. Chang. Biol.* **2015**, *21*, 4196–4209. [[CrossRef](#)] [[PubMed](#)]
- Ma, X.; Zhao, C.; Yan, W.; Zhao, X. Influences of 1.5 °C and 2.0 °C global warming scenarios on water use efficiency dynamics in the sandy areas of northern China. *Sci. Total. Environ.* **2019**, *664*, 161–174. [[CrossRef](#)]
- Ren, S.; Yi, S.; Peichl, M.; Wang, X. Diverse Responses of Vegetation Phenology to Climate Change in Different Grasslands in Inner Mongolia during 2000–2016. *Remote Sens.* **2018**, *10*, 17. [[CrossRef](#)]
- Wang, L.; Chen, W. Applicability Analysis of Standardized Precipitation Evapotranspiration Index in Drought Monitoring in China. *Plateau Meteorol.* **2014**, *33*, 423–431. [[CrossRef](#)]
- Steinmann, A. Drought indicators and triggers: A stochastic approach to evaluation. *JAWRA J. Am. Water Resour. Assoc.* **2003**, *39*, 1217–1233. [[CrossRef](#)]
- Musei, S.K.; Nyaga, J.M.; Dubow, A.Z. SPEI-based spatial and temporal evaluation of drought in Somalia. *J. Arid Environ.* **2020**, *184*, 104296. [[CrossRef](#)]
- Cook, B.I.; Smerdon, J.E.; Seager, R.; Coats, S. Global warming and 21st century drying. *Clim. Dyn.* **2014**, *43*, 2607–2627. [[CrossRef](#)]
- Vicente-Serrano, S.M.; Beguería, S.; López-Moreno, J.I. A Multiscalar Drought Index Sensitive to Global Warming: The Standardized Precipitation Evapotranspiration Index. *J. Clim.* **2010**, *23*, 1696–1718. [[CrossRef](#)]
- Rodrigues, M.; Jiménez-Ruano, A.; Peña-Angulo, D.; de la Riva, J. A comprehensive spatial-temporal analysis of driving factors of human-caused wildfires in Spain using Geographically Weighted Logistic Regression. *J. Environ. Manag.* **2018**, *225*, 177–192. [[CrossRef](#)]
- Caetano, J.M.; Tessarolo, G.; De Oliveira, G.; Souza, K.D.S.E.; Diniz-Filho, J.A.F.; Nabout, J.C. Geographical patterns in climate and agricultural technology drive soybean productivity in Brazil. *PLoS ONE* **2018**, *13*, e0191273. [[CrossRef](#)] [[PubMed](#)]
- Vicente-Serrano, S.M.; Beguería, S.; Lorenzo-Lacruz, J.; Camarero, J.J.; Lopez-Moreno, I.; Azorin-Molina, C.; Revuelto, J.; Morán-Tejeda, E.; Sanchez-Lorenzo, A. Performance of Drought Indices for Ecological, Agricultural, and Hydrological Applications. *Earth Interact.* **2012**, *16*, 1–27. [[CrossRef](#)]

13. Drumond, A.; Gimeno, L.; Nieto, R.; Trigo, R.M.; Vicente-Serrano, S.M. Drought episodes in the climatological sinks of the Mediterranean moisture source: The role of moisture transport. *Glob. Planet. Chang.* **2017**, *151*, 4–14. [[CrossRef](#)]
14. Hao, C.; Zhang, J.; Yao, F. Combination of multi-sensor remote sensing data for drought monitoring over Southwest China. *Int. J. Appl. Earth Obs. Geoinf.* **2015**, *35*, 270–283. [[CrossRef](#)]
15. Jin, L.; Wang, Y. The Impact of Drought on Biomass of Forage Grass in Hulunbuir Grassland. *Chin. J. Grassl.* **2020**, *42*, 80–90. [[CrossRef](#)]
16. Li, J.; He, Q.; Yao, J.; Hu, W. The characteristics of climate change and the impact factors analysis in the western part of Inner Mongolia. *J. Arid. Land Resour. Environ.* **2014**, *28*, 186–191. [[CrossRef](#)]
17. Tang, Q.; Liu, Y.; Zhang, C.; Su, F.; Li, Y.; Gao, Y.; Li, W.; Chen, D. Research progress on moisture source change of precipitation over the Tibetan Plateau and its surrounding areas. *Trans. Atmos. Sci.* **2020**, *43*, 1002–1009. [[CrossRef](#)]
18. Bailing, M.; Zhiyong, L.; Cunzhu, L.; Lixin, W.; Chengzhen, J.; Fuxiang, B.; Chao, J. Temporal and spatial heterogeneity of drought impact on vegetation growth on the Inner Mongolian Plateau. *Rangel. J.* **2018**, *40*, 113. [[CrossRef](#)]
19. An, Q.; He, H.; Nie, Q.; Cui, Y.; Gao, J.; Wei, C.; Xie, X.; You, J. Spatial and Temporal Variations of Drought in Inner Mongolia, China. *Water* **2020**, *12*, 1715. [[CrossRef](#)]
20. Pei, Z.; Fang, S.; Wang, L.; Yang, W. Comparative Analysis of Drought Indicated by the SPI and SPEI at Various Timescales in Inner Mongolia, China. *Water* **2020**, *12*, 1925. [[CrossRef](#)]
21. Tong, S.; Lai, Q.; Zhang, J.; Bao, Y.; Lusi, A.; Ma, Q.; Li, X.; Zhang, F. Spatiotemporal drought variability on the Mongolian Plateau from 1980–2014 based on the SPEI-PM, intensity analysis and Hurst exponent. *Sci. Total. Environ.* **2018**, *615*, 1557–1565. [[CrossRef](#)] [[PubMed](#)]
22. Qin, Y.; Zhang, T.; Yi, G.; Wei, P.; Yang, D. Remote sensing monitoring and analysis of influencing factors of drought in Inner Mongolia growing season since 2000. *J. Nat. Resour.* **2021**, *36*, 459–475. [[CrossRef](#)]
23. Yang, Z.; Ning, L.; Jidong, W. Analysis of Drought and its Possible Causes in Inner Mongolia Region for Nearly 30 Years. *J. Catastrophol.* **2013**, *28*, 67–73.
24. Psilovikos, A.; Tzimopoulos, C. Comparison of quadratic and non-linear programming (QP and NLP) optimization models in groundwater management. *J. Hydroinformatics* **2004**, *6*, 175–185. [[CrossRef](#)]
25. Zhu, L.; Meng, J.; Zhu, L. Applying Geodetector to disentangle the contributions of natural and anthropogenic factors to NDVI variations in the middle reaches of the Heihe River Basin. *Ecol. Indic.* **2020**, *117*, 106545. [[CrossRef](#)]
26. Wen, Q.; Sun, P.; Zhang, Q.; Yao, R. A multi-scalar drought index for global warming: The non-stationary standardized precipitation evaporation index (NSPEI) and spatio-temporal patterns of future drought in China. *Acta Geogr. Sin.* **2020**, *75*, 1465–1482. [[CrossRef](#)]
27. Zhu, X.; Huang, C.; Wu, B.; Su, H.; Jiao, W.; Zhang, L. Research on remote sensing drought monitoring by considering spatial non-stationary characteristics. *Natl. Remote Sens. Bull.* **2019**, *23*, 487–500. [[CrossRef](#)]
28. Zhang, P.; Yang, D.; Zhang, Y.; Li, Y.; Liu, Y.; Cen, Y.; Zhang, W.; Geng, W.; Rong, T.; Liu, Y.; et al. Re-examining the drive forces of China's industrial wastewater pollution based on GWR model at provincial level. *J. Clean. Prod.* **2020**, *262*, 121309. [[CrossRef](#)]
29. Yang, Y.; Yang, X.; He, M.; Christakos, G. Beyond mere pollution source identification: Determination of land covers emitting soil heavy metals by combining PCA/APCS, GeoDetector and GIS analysis. *CATENA* **2019**, *185*, 104297. [[CrossRef](#)]
30. Wang, J.; Xu, C. Geodetector: Principle and prospective. *Acta Geogr. Sin.* **2017**, *73*, 219–231. [[CrossRef](#)]
31. He, D.; Yi, G.; Zhang, T.; Miao, J.; Li, J.; Bie, X. Temporal and Spatial Characteristics of EVI and Its Response to Climatic Factors in Recent 16 years Based on Grey Relational Analysis in Inner Mongolia Autonomous Region, China. *Remote Sens.* **2018**, *10*, 961. [[CrossRef](#)]
32. Dobson, J.E.; Bright, E.A.; Coleman, P.R.; Durfee, R.C.; Worley, B.A. LandScan: A Global Population Database for Estimating Populations at Risk. *Photogramm. Eng. Remote Sens.* **2000**, *66*, 849–857.
33. Yin, H.; Pflugmacher, D.; Li, A.; Li, Z.; Hostert, P. Land use and land cover change in Inner Mongolia—Understanding the effects of China's re-vegetation programs. *Remote Sens. Environ.* **2018**, *204*, 918–930. [[CrossRef](#)]
34. Ming, B.; Guo, Y.; Tao, H.; Liu, G.; Li, S.; Wang, P. SPEIPM-based research on drought impact on maize yield in North China Plain. *J. Integr. Agric.* **2015**, *14*, 660–669. [[CrossRef](#)]
35. Luong, N.; Hiep, N.; Bui, T. Investigating the Spatio-Temporal Variation of Soil Moisture and Agricultural Drought towards Supporting Water Resources Management in the Red River Basin of Vietnam. *Sustainability* **2021**, *13*, 4926. [[CrossRef](#)]
36. Yang, S.; Quan, Q.; Liang, W.; Liu, T. Characteristics of Agricultural Droughts and Spatial Stratified Heterogeneity and Dependence of Dominant Factors in Inner Mongolia Autonomous Region, China. *Atmosphere* **2021**, *12*, 1249. [[CrossRef](#)]
37. Reiche, M.; Funk, R.; Zhang, Z.; Hoffmann, C.; Reiche, J.; Wehrhan, M.; Li, Y.; Sommer, M. Application of satellite remote sensing for mapping wind erosion risk and dust emission-deposition in Inner Mongolia grassland, China. *Grassl. Sci.* **2012**, *58*, 8–19. [[CrossRef](#)]
38. Jia, Y.; Cui, X.; Liu, Y.; Liu, Y.; Xu, C.; Li, T.; Ran, Q.; Wang, Y. Drought vulnerability assessment in Inner Mongolia. *Acta Ecol. Sin.* **2020**, *40*, 9070–9082. [[CrossRef](#)]
39. Fotheringham, A.S.; Charlton, M.E.; Brunsdon, C. Geographically Weighted Regression: A Natural Evolution of the Expansion Method for Spatial Data Analysis. *Environ. Plan. A* **1998**, *30*, 1905–1927. [[CrossRef](#)]

40. Alsafadi, K.; Al-Ansari, N.; Mokhtar, A.; Mohammed, S.; Elbeltagi, A.; Sammen, S.S.; Bi, S. An evapotranspiration deficit-based drought index to detect variability of terrestrial carbon productivity in the Middle East. *Environ. Res. Lett.* **2022**, *17*, 014051. [[CrossRef](#)]
41. Piao, S.; Friedlingstein, P.; Ciais, P.; Zhou, L.; Chen, A. Effect of climate and CO₂ changes on the greening of the Northern Hemisphere over the past two decades. *Geophys. Res. Lett.* **2006**, *33*, L23402. [[CrossRef](#)]
42. Zhang, R.; Zhao, X.; Zuo, X.; Degen, A.A.; Li, Y.; Liu, X.; Luo, Y.; Qu, H.; Lian, J.; Wang, R. Drought-induced shift from a carbon sink to a carbon source in the grasslands of Inner Mongolia, China. *CATENA* **2020**, *195*, 104845. [[CrossRef](#)]
43. Qiu, G.Y.; Xie, F.; Feng, Y.C.; Tian, F. Experimental studies on the effects of the “Conversion of Cropland to Grassland Program” on the water budget and evapotranspiration in a semi-arid steppe in Inner Mongolia, China. *J. Hydrol.* **2011**, *411*, 120–129. [[CrossRef](#)]
44. Jin, L.; Zhang, J.; Wang, R.; Bao, Y.; Guo, E. Analysis for Spatio-Temporal Variation Characteristics of Droughts in Different Climatic Regions of the Mongolian Plateau Based on SPEI. *Sustainability* **2019**, *11*, 5767. [[CrossRef](#)]
45. Brueck, H.; Erdle, K.; Gao, Y.; Giese, M.; Zhao, Y.; Peth, S.; Lin, S. Effects of N and water supply on water use-efficiency of a semiarid grassland in Inner Mongolia. *Plant Soil.* **2010**, *328*, 495–505. [[CrossRef](#)]
46. Pan, T.; Wu, S.; He, D.; Dai, E.; Liu, Y. Ecological Effects of Longitudinal Range-Gorge Land Surface Pattern and Its Regional Differentiation. *Acta Geogr. Sin.* **2012**, *67*, 13–26. [[CrossRef](#)]
47. An, C.-B.; Chen, F.-H.; Barton, L. Holocene environmental changes in Mongolia: A review. *Glob. Planet. Chang.* **2008**, *63*, 283–289. [[CrossRef](#)]
48. Ukkola, A.M.; Prentice, I.C.; Keenan, T.F.; Van Dijk, A.I.; Viney, N.R.; Myneni, R.B.; Bi, J. Reduced streamflow in water-stressed climates consistent with CO₂ effects on vegetation. *Nat. Clim. Chang.* **2016**, *6*, 75–78. [[CrossRef](#)]
49. Mu, S.; Li, J.; Chen, Y.; Gang, C.; Zhou, W.; Ju, W. Spatial Differences of Variations of Vegetation Coverage in Inner Mongolia during 2001–2010. *Acta Geogr. Sin.* **2012**, *67*, 1255–1268.
50. Shi, H.; Yang, S.; Li, R.; Li, X.; Li, W.; Yan, J.; Miao, Q.; Li, Z. Water-Saving Irrigation and Utilization Efficiency of Water and Fertilizer in Hetao Irrigation District of Inner Mongolia: Prospect for Future Research. *J. Irrig. Drain.* **2020**, *39*, 1–12. [[CrossRef](#)]
51. Dregne, H.E. Desertification of Arid Lands. *Econ. Geogr.* **1977**, *53*, 322–331. [[CrossRef](#)]
52. Julich, S.; Moorcroft, M.-A.; Feger, K.; van Tol, J. The impact of overgrazing on water fluxes in a semi-arid watershed—The suitability of watershed scale modeling in a data scarce area. *J. Hydrol. Reg. Stud.* **2022**, *43*, 101178. [[CrossRef](#)]
53. Shrestha, A.; Luo, W. Analysis of Groundwater Nitrate Contamination in the Central Valley: Comparison of the Geodetector Method, Principal Component Analysis and Geographically Weighted Regression. *ISPRS Int. J. Geo-Inf.* **2017**, *6*, 297. [[CrossRef](#)]
54. Zhao, R.; Zhan, L.; Yao, M.; Yang, L. A geographically weighted regression model augmented by Geodetector analysis and principal component analysis for the spatial distribution of PM_{2.5}. *Sustain. Cities Soc.* **2020**, *56*, 102106. [[CrossRef](#)]